THE ASTROPHYSICAL JOURNAL, 562:950–956, 2001 December 1

THE *BeppoSAX* 0.1–100 keV SPECTRUM OF THE X-RAY PULSAR 4U 1538−52

N. R. ROBBA,[1] L. BURDERI,[2] T. DI SALVO,[1,3] R. IARIA,[1] AND G. CUSUMANO[4]

Received 2000 September 21; accepted 2001 August 6

ABSTRACT

We report the results of temporal and spectral analysis performed on the X-ray pulsar 4U 1538−52 observed by *BeppoSAX*. We obtained a new estimate of the spin period of the neutron star $P = 528.24 \pm 0.01$ s (corrected for the orbital motion of the X-ray source): the source is still in the spin-up state, as it has been since 1988. The pulse profile is double peaked, although significant variations of the relative intensity of the peaks with energy are present. The broadband (0.12–100 keV) out-of-eclipse spectrum is well described by an absorbed power law modified by a high-energy cutoff at ∼16 keV (*e*-folding energy ∼10 keV) plus an iron emission line at ∼6.4 keV. A cyclotron line at ∼21 keV is present. The width of the line is consistent with thermal Doppler broadening at the temperature of the exponential cutoff. We searched for the presence of the second harmonic, previously reported for this source. We found no evidence of lines at ∼42 keV, although an absorption feature at 51 keV seems to be present (at 99% confidence level). A soft excess, modeled by a blackbody with a temperature of ∼0.08 keV could be present, probably emitted by the matter at the magnetosphere. We also performed a spectral analysis during the X-ray eclipse. The spectral evolution during the eclipse can be well described by a progressive covering of the primary Comptonization spectrum that is scattered into the line of sight. During the deep eclipse this spectrum also softens, suggesting that the dust-scattered component becomes important. An alternative, more complex model, with an emission iron line and scattered components (as the one that has been used to fit the eclipse of Cen X-3), also gives a good fit of the deep-eclipse data.

Subject headings: pulsars: general — stars: individual (4U 1538−52) — stars: neutron — X-rays: stars

1. INTRODUCTION

4U 1538−52 is a wind-fed X-ray binary system formed by a massive (17 $M_\odot$) B0 star and a neutron star spinning with a period of about 529 s (Davison 1977; Becker et al. 1977). The X-ray luminosity has been estimated $\sim 2 \times 10^{36}$ ergs s^{-1} for a distance of ∼6.4 kpc (Becker et al. 1977). The orbit, in an almost edge-on plane, is characterized by a period of 3.75 days, a low eccentricity of ∼0.08, and a well-defined X-ray eclipse lasting ∼0.6 days (Davison 1977; Becker et al. 1977). Pulse period measurements show that the neutron star was in a spin-down state before 1988, with $|\dot{P}/P| \sim 10^{-11}$ s^{-1}, and in a spin-up state with the same $|\dot{P}/P|$ after 1988 (Rubin et al. 1997).

Before the first *Ginga* observation (Clark et al. 1990), the X-ray spectrum of 4U 1538−52 had been well modeled by a power law modified by a high-energy exponential cutoff and an iron emission line at 6.7 keV (equivalent width EW ∼ 100 eV). A phase-dependent absorption feature around 20 keV was observed in the X-ray spectrum by *Ginga* (Clark et al. 1990) and was explained as cyclotron resonance absorption. A cutoff in the spectrum starting at ∼30 keV was interpreted as the second harmonic, but the *Ginga* energy range precluded any definitive conclusion. A fit of the energy-dependent pulse profiles in the range 10–38 keV to theoretical models of the pulsar emission has been performed by Bulik et al. (1992, 1995). The results are in agreement with pencil emission from a strongly magnetized, optically thick ($\tau \sim 20$), short ($h \ll R_{NS}$) slab of plasma, heated by a Coulomb collision stopping mechanism in the accreting matter, in line with theoretical calculations of Meszaros & Nagel (1985a, 1985b) and Brainerd & Meszaros (1991) for the nonrelativistic and the relativistic cases, respectively. More recently, Makishima et al. (1999), in a paper discussing *Ginga* observations of a number of X-ray pulsators, briefly reported the results of an analysis of a 3–60 keV *Ginga* spectrum acquired during an observation on 1991 July 27. They fitted the continuum with the so-called NPEX model (Mihara 1995) that is the sum of two power laws, of negative and positive index, respectively, both multiplied by an exponential cutoff of thermal origin. A cyclotron feature at ∼20 keV was fitted by a pseudo-Lorentzian shape (i.e., a Lorentzian multiplied by the energy squared; Mihara 1995). With this model they obtained a value of the χ^2/degrees of freedom (dof) of 46/29.

In this paper we present for the first time a broadband (0.12–100 keV) spectrum of 4U 1538−52. We clearly show that this spectrum can be well fitted only if a thermal cutoff and a cyclotron absorption feature at ∼21 keV are included in the model. We also do not find strong evidence of a second harmonic at ∼42 keV, although a weak feature could be present at a slightly higher energy.

2. OBSERVATIONS AND TEMPORAL ANALYSIS

BeppoSAX observed 4U 1538−52 with its Narrow Field Instruments (NFIs; Boella et al. 1997) in 1998 from July 29 to August 1. The NFIs are four coaligned instruments with a broadband coverage from 0.1 up to 200 keV, with good spectral resolution in the whole range. The Low Energy

[1] Dipartimento di Scienze Fisiche ed Astronomiche, Università di Palermo, via Archirafi 36, 90123 Palermo, Italy; robba@gifco.fisica.unipa.it.

[2] Osservatorio Astronomico di Roma, Via Frascati 33, 00040 Monteporzio Catone, Roma, Italy.

[3] Astronomical Institute Anton Pannekoek, University of Amsterdam and Center for High-Energy Astrophysics, Kruislaan 403, NL 1098 SJ Amsterdam, the Netherlands.

[4] Istituto di Fisica Cosmica con Applicazioni all'Informatica CNR, Via U. La Malfa 153, Palermo, I-90146, Italy.

Concentrator Spectrometer (LECS, energy range 0.1–10 keV) and the Medium Energy Concentrator Spectrometer (MECS, 1–11 keV) have imaging capabilities with a field of view (FOV) of 20′ and 30′ radii, respectively. We selected the data for scientific analysis in circular regions of the FOV, centered on the source, of 8′ and 4′ radii for LECS and MECS, respectively. The background subtraction is usually obtained using blank-sky observations, in which the background spectra are extracted from regions of the FOV similar to those used for the source. Because of the possibility of a contribution from the Galactic ridge at the coordinates of 4U 1538−52, we paid particular attention to the background estimation. This is particularly important for the spectral analysis during the eclipse, when the source flux is at a very low level. Local background has been therefore measured in a region of the image 16′ and 20′ far from the source for LECS and MECS, respectively, and compared with the background of the archive blank fields. LECS and MECS local background spectrum is compatible with the blank-field spectrum, and therefore blank-sky background, which has better statistics, has been used. The High Pressure Gas Scintillator Proportional Counter (HPGSPC, 7–60 keV) and the Phoswich Detector System (PDS, 13–300 keV) do not have imaging capabilities, and their FOVs of $\sim 1^\circ$ FWHM are delimited by collimators. The background subtraction for these instruments is obtained using off-source data accumulated during the rocking of the collimators. The energy ranges used in the spectral analysis for the NFIs are 0.12–4 keV for the LECS, 1.8–10.5 keV for the MECS, 8–30 keV for the HPGSPC, and 15–100 keV for the PDS. To take into account intercalibration systematics, different normalizations of the NFIs are considered in the spectral analysis by including normalizing factors, fixed to 1 for the MECS, and kept free for the other instruments. A systematic error of 1% was added to all the spectra, although, for this relatively weak flux, it is negligible when compared to the statistical error.

Figure 1 shows the 4U 1538−52 light curve, binned at 5700 s, in four different energy bands: 0.1–2.5 keV (LECS data), 3–5 keV (MECS data), 5–10 keV (MECS data), and 15–200 keV (PDS data). This light curve shows the source in its eclipse state during the first ~ 52 ks and out of eclipse in the last ~ 177 ks. A dip, probably owing to low-energy absorption, is also present in the 0.1–2.5 keV light curve. Adopting a distance of 6.4 kpc (Becker et al. 1977) and the spectral model described in § 3 (see Table 1), we derived the source luminosity out of eclipse, which is $\sim 1.8 \times 10^{36}$ ergs s^{-1} in the energy range 2–10 keV and $\sim 4.7 \times 10^{36}$ ergs s^{-1} in the whole range 0.1–100 keV.

We performed a temporal analysis on the out-of-eclipse data to search for the pulse period of the source using MECS data, which have the best statistics. The arrival times of all the events were reported to the solar system barycenter. We corrected the arrival times for the orbital motion of the source adopting the orbital parameters reported by Rubin et al. (1997), $P_{\rm orb} = 3.72839 \pm 0.00002$ days and $a \sin i = 53.5 \pm 1.4$ lt-s, and neglecting the eccentricity because of its low value. From the MECS data we estimated that the center-of-eclipse time is $T_{\rm ecl} = 51024.460 \pm 0.032$ MJD. With these values we corrected the event times according to the formula:

$$\Delta t = (a \sin i) \cos\left[\frac{2\pi(t - T_{\rm ecl})}{P_{\rm orb}}\right].$$

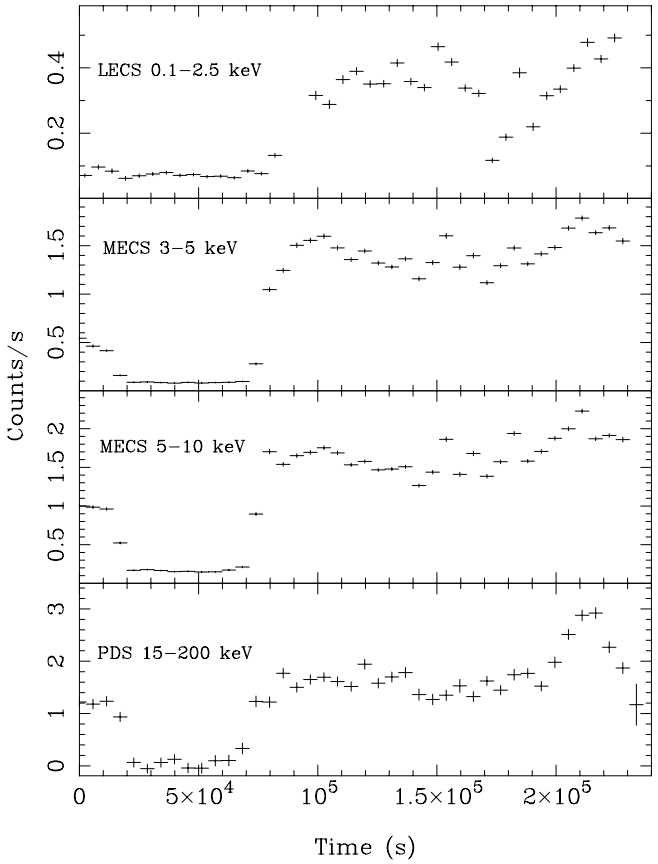

FIG. 1.—4U 1538−52 light curve, binned at 5700 s, in four different energy bands: 0.1–2.5 keV (LECS data), 3–5 keV (MECS data), 5–10 keV (MECS data), 15–200 keV (PDS data).

Then we performed a folding search for the best pulse period on these corrected arrival times. The best period obtained was 528.24 ± 0.01 s, demonstrating that the source is still in a spin-up state. We checked the orbital correction a posteriori dividing the whole data set into consecutive intervals, which we folded using the spin period derived above. No phase shifts were observed between these intervals.

Figure 2 shows the pulse profiles during out-of-eclipse intervals in different energy bands, namely, 0.1–1.8 keV (LECS, *upper panel*), 1.8–10.5 keV (MECS, *middle panel*), 15–100 keV (PDS, *lower panel*). A double-peaked pulse profile is present in the 1.8–10 keV band. The secondary peak is asymmetric in this energy range, and the primary peak is broad and shows some structures at its maximum. The secondary peak is absent in the soft range 0.1–1.8 keV, while the primary peak still shows notchlike structures at its maximum. In the PDS range (15–100 keV) the emission is still pulsed, with the secondary peak less pronounced and more symmetric and the primary peak narrower and smooth. We have also produced PDS folded light curves in the following energy ranges: 15–20 keV (below the cyclotron line energy; see Clark et al. 1990 and § 3.1 in this paper), 20–30 keV (around the cyclotron line energy), and 30–100 keV (above the cyclotron line energy). In agreement with *Ginga* results (Clark et al. 1990) we find that the secondary peak disappears at the cyclotron energy. Because of the low statistics, there is no evidence that the secondary peak reappears at energies higher than 30 keV. In Figure 3

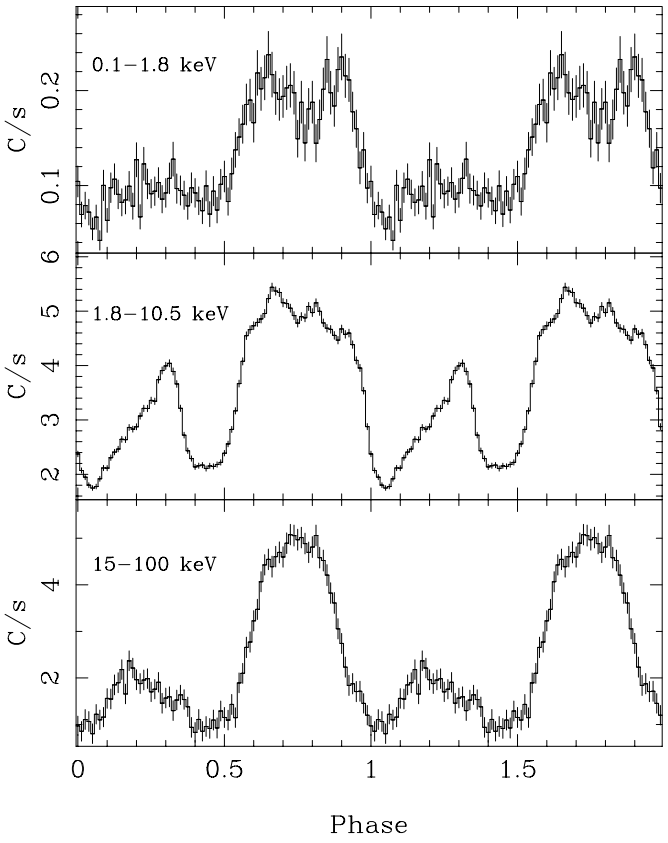

FIG. 2.—Pulse profiles during the post-egress phase in different energy bands: 0.1–1.8 keV (LECS, *upper panel*), 1.8–10.5 keV (MECS, *middle panel*), and 15–100 keV (PDS, *lower panel*).

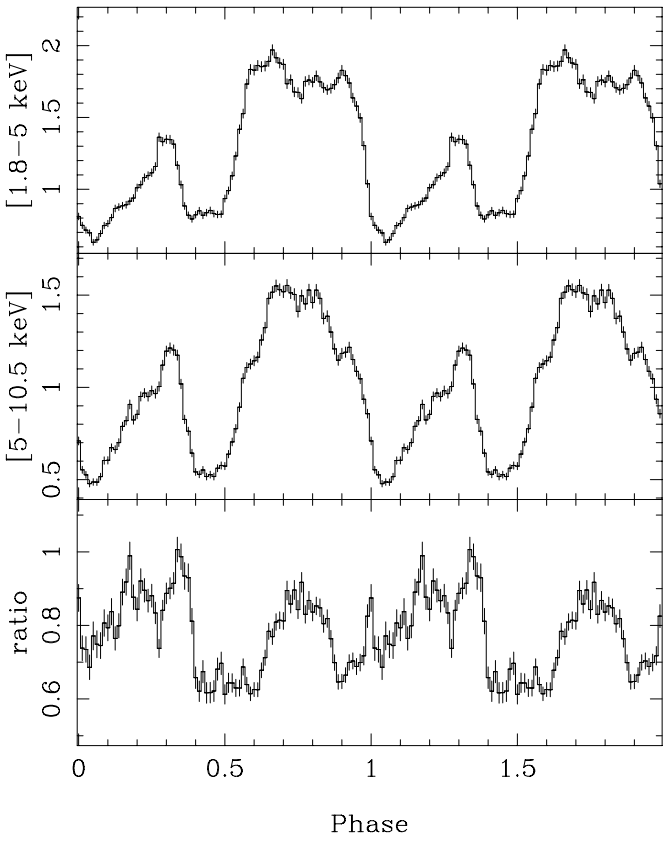

FIG. 3.—MECS folded light curves in the energy ranges 1.8–5 keV (*upper panel*) and 5–10.5 keV (*middle panel*), and their hardness ratio (*lower panel*).

we plotted the MECS folded light curves in the energy ranges 1.8–5 keV and 5–10.5 keV and their hardness ratio. Several structures are visible in this ratio, demonstrating the high spectral variability of the emission with the pulse phase.

3. SPECTRAL ANALYSIS

3.1. *Pulse-Phase–Averaged Spectrum*

We performed spectral analysis on the post-egress energy spectrum of 4U 1538−52 in the energy range 0.12–100 keV. The high-energy part of the spectrum (above $\sim$10 keV) is not well fitted by a power law modified by two absorption features as proposed by Clark et al. (1990) in the analysis of *Ginga* data. The broader band of the *BeppoSAX* instruments unambiguously demonstrates that an absorption feature and an exponential cutoff are needed to adequately model the spectrum.

We fit the spectrum with an absorbed power-law continuum modified by a high-energy cutoff and by an absorption cyclotron line of Gaussian shape plus a Gaussian emission line at $\sim$6.4 keV owing to fluorescence of iron in low-ionization stages. The model used to fit the cyclotron line is a multiplicative Gaussian of the form: 1 − Depth exp $[-(E - E_{\rm cyc})^2/(2\sigma_{\rm cyc}^2)]$. This model gave a good fit with a χ^2/dof = 453/421. The best-fit parameters are shown in Table 1; the observed spectrum and the residuals (in units of σ) are shown in Figure 4 (*upper and middle panels*, respectively). With respect to this model, residuals are still visible in the soft energy range, below $\sim$1 keV, and in the PDS range, between 40 and 60 keV. Since the latter is the range of energy in which we expect to find harmonics of the cyclotron line, we first added a cyclotron line fixing the energy at twice the fundamental; this did not improve the fit. Therefore, we let the cyclotron line energy vary. In this way we obtain a reduction of the χ^2 to 442/418. An *F*-test gives a probability of chance improvement of 1%. The energy of the second absorption line is 51^{+4}_{-3} keV, its depth is $0.9^{+0.1}_{-0.4}$, and its width is 3.3^{+5}_{-1} keV. The residuals with respect to this model, containing two cyclotron lines, are shown in Figure 4 (*lower panel*). As is visible in this figure, some residuals remain in the soft energy range, below 1 keV. The addition of a soft blackbody to the model reported in Table 1 improves the fit, giving χ^2/dof = 433/419, corresponding to a probability of chance improvement of $\sim 8.4 \times 10^{-3}$. The blackbody has a temperature of 0.08 ± 0.04 keV and a luminosity of $\sim 1.6 \times 10^{37}$ ergs s^{-1} (although this last parameter is not well constrained by the data and ranges between 1.3×10^{36} and 7.6×10^{39} ergs s^{-1}). Moreover, the spectral model for the soft excess is not univocally determined: a bremsstrahlung component with a temperature of 0.10 ± 0.07 keV gives an equally good fit.

We also tried the so-called NPEX model to fit the continuum. This model has been successfully used to fit the continuum of a number of high-mass X-ray binaries (Mihara 1995; Makishima et al. 1999) and consists of a negative plus a positive power law with a common exponential cutoff. It approximates the spectrum produced by unsaturated thermal Comptonization in a plasma of temperature *T*. Using NPEX together with the absorption cyclotron feature (modeled by a pseudo-Lorentzian shape) and the iron emission line, we obtain a negative photon index of 0.59 ± 0.07 and a temperature of 4.93 ± 0.07 keV, with the positive photon index fixed to 2. In this case we obtained a

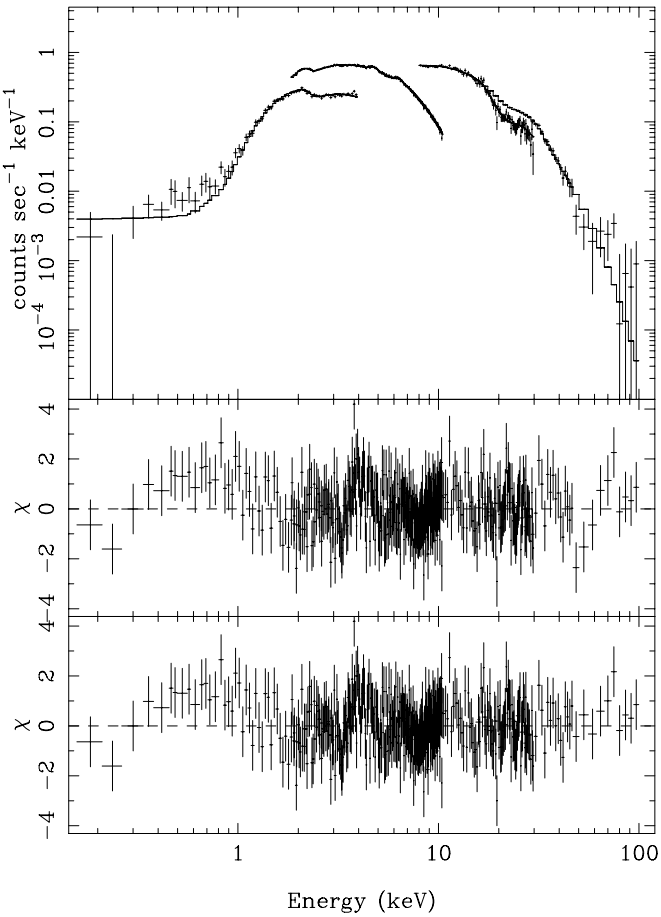

FIG. 4.—Broadband spectrum of 4U 1538−52 (*upper panel*), residuals, in units of σ, with respect to the best-fit model shown in Table 1 (*middle panel*), and residuals, in units of σ, with respect to the model with two cyclotron lines (*lower panel*).

χ^2/dof = 463/419, which is not better than the previous model (see. Table 1). The residuals in the soft band (below 1 keV) and in the hard range (around 50 keV) are still visible.

3.2. *Pulse-Phase–Resolved Spectra*

The hardness ratio shown in Figure 3 indicates the presence of significant variations of the spectrum with the pulse phase. To investigate these variations we have divided the pulse profile in four phase intervals: 0–0.5, corresponding to the secondary peak; 0.5–0.65, corresponding to the rising phase of the primary peak; 0.65–0.75, corresponding to the maximum of the primary peak; 0.75–1, corresponding to the descent phase of the primary peak (see Fig. 2). We produced energy spectra corresponding to each of these phase intervals, which were fitted by the same model used to fit the pulse-phase–averaged spectrum, i.e., a power law with high-energy cutoff, the iron emission line, and the absorption cyclotron line. The results are reported in Table 1.

The energy of the cyclotron line varies between 20.8 keV at the primary-peak maximum and 22.8 keV in the rising phase of the primary peak, although these variations are not highly significant when compared to the associated error bars. More significant variations are observed in the depth and width of the cyclotron line. In particular, the depth is larger when the flux is lower, while the width of the line reaches its maximum and minimum values in the rising and descent phase of the primary peak, respectively. Other significant variations with the pulse phase are in the shape of the continuum. In particular, the power law is flatter in correspondence of the primary and secondary peaks, while it is steeper at the other phase intervals. The energy of the cutoff seems also to be lower in correspondence of the primary and secondary peaks, while no clear variation is present in the *e*-folding energy. Finally, the iron emission line is compatible with being unchanged along the pulse profile, although it seems to be weaker in the rising phase and at the maximum of the primary peak. No statistically significant residuals are observed in the energy range between 40 and 50 keV, and therefore no second cyclotron harmonic is required to fit these spectra, although this could be due to the lower statistics of the phase-resolved spectra with respect to the averaged spectrum. Residuals below 1 keV are visible in the spectra at phases 0–0.5 and 0.75–1. In these cases the addition of a soft blackbody gives a prob-

TABLE 1

RESULTS OF THE FIT OF THE PULSE-PHASES–SELECTED AND –AVERAGED SPECTRA IN THE ENERGY RANGE 0.1–100 KEV

	PHASE				
PARAMETER	0–0.5	0.5–0.65	0.65–0.75	0.75–1	Averaged
N_H ($\times 10^{22}$ cm^{-2}).....	1.70 ± 0.07	1.8 ± 0.1	1.4 ± 0.1	1.58 ± 0.08	1.63 ± 0.04
P.I.....	1.06 ± 0.02	1.39 ± 0.04	0.97 ± 0.03	1.12 ± 0.02	1.12 ± 0.01
N ($\times 10^{-2}$).....	2.6 ± 0.1	6.6 ± 0.4	4.3 ± 0.2	4.8 ± 0.2	3.8 ± 0.8
E_{cut} (keV)	16 ± 1	25 ± 3	14 ± 1	17 ± 1	16.4 ± 0.7
E_{fold} (keV)	7.8 ± 0.8	10.3 ± 2	11.9 ± 0.9	9.3 ± 0.7	10.0 ± 0.5
E_{cyc} (keV)	21.1 ± 0.3	22.8 ± 1	20.8 ± 0.6	21.5 ± 0.5	21.1 ± 0.2
Depth	0.69 ± 0.06	0.56 ± 0.02	0.36 ± 0.07	0.37 ± 0.07	0.49 ± 0.04
σ_{cyc} (keV)	3.7 ± 0.4	5.6 ± 1.4	3.6 ± 0.8	$2.5^{+0.6}_{-0.8}$	3.4 ± 0.3
E_{Fe} (keV).....	6.44 ± 0.06	6.4 (frozen)	6.4 (frozen)	6.38 ± 0.09	6.37 ± 0.05
σ_{Fe} (keV).....	0.0 (frozen)	0.0 (frozen)	0.0 (frozen)	0.0 (frozen)	0.0 (frozen)
I_{Fe} ($\times 10^{-4}$).....	3 ± 1	< 3	< 2.3	$2.8^{+1}_{-0.8}$	2.5 ± 0.5
EW_{Fe} (eV)	85	< 43	< 52	57	53
Flux	6.46	9.97	16.4	12.5	9.60
χ^2/dof	483/495	391/394	374/371	504/467	453/421

NOTE.—Uncertainties are at the 90% confidence level for a single parameter. The power-law normalization, N, is in units of ph keV^{-1} cm^{-2} s^{-1} at 1 keV. The Gaussian emission line intensity, I_{Fe}, is in units of ph cm^{-2} s^{-1}. The flux, in units of 10^{-10} ergs cm^{-2} s^{-1}, is calculated in the 0.1–100 keV energy range.

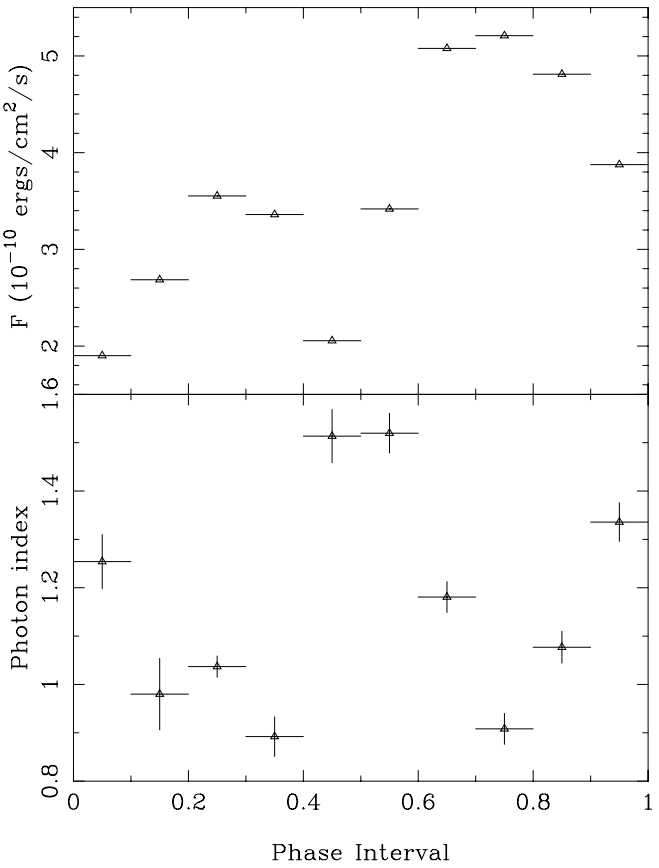

FIG. 5.—Measured photon index (*lower panel*) and the corresponding flux in the 2–10 keV energy band (*upper panel*) reported vs. the corresponding phase interval.

ability of chance improvement of the fit of 0.02% and 0.08%, respectively. The temperatures of this component were 0.032 ± 0.006 and 0.10 ± 0.04 keV, respectively.

To better investigate the variation of the power-law photon index with the pulse phase, we divided the pulse profile in 10 intervals and produced energy spectra from LECS and MECS data (for which the statistics is the highest) for each of these intervals. These spectra were fitted by a power law and a Gaussian emission line, with photoelectric absorption. The measured photon index is reported versus the corresponding phase interval in Figure 5 (*lower panel*) together with the corresponding flux in the 2–10 keV energy band (*upper panel*). As can be seen from this figure, there is a clear anticorrelation between the photon index and the flux, with the spectrum being flatter in correspondence with higher flux levels.

3.3. *Spectral Evolution during the Eclipse*

The eclipse of the X-ray source is clearly visible at the beginning of the *BeppoSAX* observation (see Fig. 1). To study the spectral evolution during the eclipse, we considered the MECS spectra corresponding to the following three intervals. The first interval (the ingress) corresponds to the first 20 ks of the light curve, during which the soft (0.1–2.5 keV) emission was already at its minimum, while some hard emission is clearly visible in the MECS and PDS light curves. The second interval (the deep eclipse) corresponds to the 50 ks in which the flux of the source was at its minimum in all the energy bands. The third interval (the egress) corresponds to the successive 20 ks in which the source gradually came back to its normal flux level. The spectra were rebinned in order to have at least 30 counts in each energy bin.

These spectra cannot be fitted by a simple power law with photoelectric absorption: the main features in the residuals are a soft excess below ~ 3 keV and a prominent excess between 6 and 7 keV. We therefore fitted these spectra with the same model used for the averaged spectrum out of eclipse (i.e., a power law, a Gaussian emission line, and the Galactic photoelectric absorption; see Table 1) multiplied by a partial covering component. In this model, the Galactic hydrogen column $N_{\rm H}$, the power-law photon index, and the emission line parameters were fixed to the values found for the averaged out-of-eclipse spectrum, while the partial covering parameters, i.e., the equivalent hydrogen column $N_{\rm Hpc}$ and the covering fraction $f_{\rm pc}$, as well as the power-law normalization were considered free parameters in the fit. This model could well fit the ingress and egress spectra but gave a poor fit to the deep-eclipse spectrum, for which we obtained a $\chi^2/{\rm dof} = 235/58$. The main feature in the residuals was a soft excess below ~ 3 keV. We obtained a significant improvement of the fit allowing the power-law photon index to vary. The best-fit value of this parameter was ~ 2.6, and the corresponding $\chi^2/{\rm dof}$ was 74/57. The results of these fits are reported in Table 2, and the unfolded spectra are shown in Figure 6.

We also tried to fit these spectra with a more complex model for the continuum, i.e., the model that has been suggested to explain the emission during the eclipse in Cen X-3 (e.g., Nagase et al. 1992; Ebisawa et al. 1996). This model consists of three components: the direct component from the neutron star, the electron-scattered component from the circumstellar matter, and the dust-scattered component

TABLE 2

RESULTS OF THE FIT OF THE SPECTRA DURING THE ECLIPSE IN THE ENERGY RANGE 1.8–10 keV

Parameter	Ingress	Eclipse	Egress
$N_{\rm H}$	1.63 (frozen)	1.63 (frozen)	1.63 (frozen)
P.I.	1.12 (frozen)	$2.68^{+0.2}_{-0.1}$	1.12 (frozen)
Norm	$(2.56 \pm 0.08) \times 10^{-2}$	$0.3^{+0.2}_{-0.1}$	$(3.5 \pm 0.1) \times 10^{-2}$
$N_{\rm Hpc}$	17 ± 1	140^{+30}_{-20}	8 ± 1
$f_{\rm pc}$	0.916 ± 0.009	$0.982^{+0.007}_{-0.010}$	0.80 ± 0.03
χ^2/dof.....	150/154	74/57	174/167

NOTE.—Uncertainties are at the 90% confidence level for a single parameter. The units of the spectral parameters are as defined in Table 1.

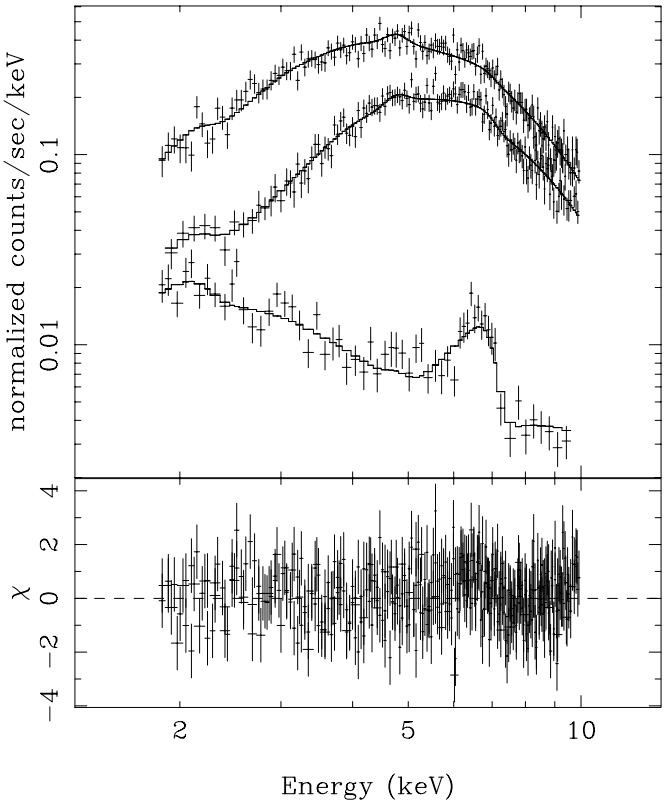

FIG. 6.—*Top panel*: Spectra of 4U 1538−52 during the ingress (*middle*), the deep eclipse (*bottom*), and the egress (*top*), together with the spectral model used to fit these spectra (see Table 2). *Bottom panel*: Corresponding residuals in units of σ.

from the interstellar dust. The first two have the same spectral shape, which we modeled with power laws with photon indices fixed to 1, but different normalizations and absorption columns. The third one is softer by approximately E^{-2} and was modeled by a power law with photon index fixed to 3. With this model we can obtain a good description of the deep-eclipse spectrum if we also add a Gaussian emission line at 6.66 keV (with $\sigma \sim 0.17$ and equivalent width ~ 4 keV), giving a $\chi^2/\mathrm{dof} = 58/53$. For the other two spectra (eclipse ingress and egress) we do not obtain a stable fit with this model, and the spectral parameters are not constrained. This is due to the fact that one of these components is indeed not required by the data and could be eliminated without affecting the results. Therefore, we prefer the previous spectral deconvolution using the partial covering, which has less free parameters and gives stable fits to all the spectra. This model can well describe both the evolution of the soft part of the spectra and the prominent feature at 6–7 keV, without the addition of extra emission components.

4. DISCUSSION AND CONCLUSIONS

We performed temporal and broadband (0.1–100 keV) spectral analysis on the out-of-eclipse and eclipse data of 4U 1538−52 observed by *BeppoSAX* NFIs. We obtained a new measurement of the spin period $P_{\mathrm{spin}} = 528.24 \pm 0.01$ s, which indicates that the neutron star is still spinning up. The pulse profile is double peaked in the MECS energy range (1.8–10.5 keV), with a main pulse and a secondary one. The secondary peak is much fainter in the high-energy range (15–100 keV) and absent in the soft energy range (0.1–1.8 keV).

The broadband energy spectrum is well fitted by a power law with high-energy cutoff continuum (the typical continuum of the X-ray pulsators), with low-energy absorption by cold matter, an emission line owing to fluorescence from iron in low-ionization stages, and an absorption feature around 20 keV, interpreted as due to cyclotron scattering (in agreement with, e.g., Clark et al. 1990). The cyclotron line parameters are similar to those measured by *Ginga* (Clark et al. 1990; Makishima et al. 1999), with small differences owing to the different models (Gaussian vs. pseudo-Lorentzian) used to fit the cyclotron line. A turnover of the spectrum above the cyclotron line energy was previously interpreted as due to the presence of the second cyclotron harmonic or a high-energy thermal cutoff (Clark et al. 1990). Makishima et al. (1999), using the NPEX model, interpreted this turnover in the spectrum as due to a thermal cutoff, although they fitted the spectrum in a relatively narrow energy range (2–60 keV) and obtained a $\chi^2/\mathrm{dof} \simeq 46/29$. The broadband capabilities of the *BeppoSAX* NFIs (0.1–100 keV) have unambiguously demonstrated that the claimed second harmonic present at the edge of the energy range of the *Ginga* LAC actually is an exponential cutoff, which we also interpret as thermal with associated temperature given by the *e*-folding energy of ~ 10 keV. If this interpretation is correct, we expect a Gaussian thermal broadening of the cyclotron absorption feature according to the formula $\sigma_{\mathrm{cyc}}/E_{\mathrm{cyc}} = (kT/m_{\mathrm{e}}c^2)^{1/2}$ (Rybicki & Lightman 1979), where $m_{\mathrm{e}}c^2$ is the rest energy of the electron. For $E_{\mathrm{cyc}} = 21$ keV and $kT = 10$ keV, we found $\sigma = 2.9$ keV, in agreement with the measured broadening of $\sigma = 3.4$ keV.

The thermal nature of the broadening of the cyclotron absorption feature seems to be the more natural interpretation for the width of these lines, although different interpretations have also been proposed. It seems possible that variations of the field strength along the accretion column could originate the variations of the broadening observed in the pulse-phase–resolved spectroscopy performed on some sources. Indeed, Bulik et al. (1995) claim that multiple field values are needed to explain the pulse-phase–resolved spectra of *Ginga* data of 4U 1538−52. Although this is still a viable possibility, we want to stress that, thanks to the broadband capabilities of the *BeppoSAX* satellite, in an increasing number of X-ray pulsators the shape of the high-energy continuum (underlying the absorption cyclotron lines) has been determined quite accurately. In particular, the presence of a power law with an exponential cutoff seems a common feature among these sources. If a multiplicative Gaussian absorption feature is used to fit the cyclotron lines a good fit has been obtained in several cases. We note that a multiplicative Gaussian shape (which is also used in this paper) can better describe the effects of thermal broadening of the cyclotron feature (as discussed in Burderi et al. 2000). As can be seen in Dal Fiume et al. (1999), there is a general agreement between the measured width of cyclotron lines in several sources and the predicted value of the width in the hypothesis of thermal broadening.

Another absorption feature might be present in the spectrum of 4U 1538−52 around 50 keV (at 99% confidence level). The presence of variations of the pulse profile at energies below and above 50 keV could provide a confirmation of the presence of a cyclotron feature at this energy. Unfortunately, although the primary peak is still observed in the folded light curve at energies above 50 keV, the reduced statistics prevent us from seeing significant variations of the

pulse profile at high energy. If confirmed, this absorption feature might be interpreted as the second harmonic of the 20 keV cyclotron line. However, the energy of this second feature (51^{+4}_{-3} keV) does not seem compatible with being double than that of the fundamental (21.1 ± 0.2 keV). This discrepancy could be explained by considering that the optical depths of the fundamental and second harmonic are different, implying that the two lines could form at different heights, where the dipolar magnetic field of the neutron star has different intensities. In particular, the fundamental, with a larger cross section, should form in the upper atmosphere where the magnetic field is weaker. We calculate that a difference in the heights of ~ 0.07 neutron star radii is sufficient to explain the difference in the cyclotron energies. Another possibility is that we see two different lines coming from the two magnetic poles. A displacement of the magnetic dipole momentum by about 0.15 neutron star radii from the center (as already detected in other X-ray pulsators, e.g., Cen X-3; Burderi et. al. 2000) is sufficient to explain the difference of energy of the two lines produced at the two magnetic poles. In this case we expect a phase dependence of the strength of these two lines. In principle, phase-resolved spectral analysis could address this question although the low statistics at the energies of the second line prevents any conclusion with the present data set. Further observations are needed to confirm the presence of the second harmonic and to address this interesting question.

We also performed a pulse-phase–resolved spectral analysis on these data, dividing the pulse profile into four intervals, corresponding to the secondary peak and the rising, maximum, and descent phases of the primary peak. The cyclotron line energy seems to vary with the pulse phase, reaching its maximum and minimum values in the rising phase and at the maximum of the primary peak, respectively, although the large error bars prevent any firm conclusion on the basis of these data. The line depth is higher at the secondary peak phase, while the width reaches its maximum and minimum values at the rising and descent phases of the primary peak, respectively. These variations are in general agreement with what is observed, with higher statistical significance, in the *Ginga* data of 4U 1538−52 (Clark et al. 1990; Bulik et al. 1992). Significant variations with the pulse phase are also observed in the continuum model. In particular, the power law is flatter at the phases of the two peaks, and the corresponding values of the cutoff energy tend to be lower than in the other phase intervals. This behavior of the photon index is better seen in Figure 5, where we show the results of the fit of 10 phase intervals in the LECS and MECS ranges. These results are similar with previous results from *EXOSAT* (Robba et al. 1992) and *Ginga* (Clark et al. 1990), and hence they probably reflect true variations of the Compton y-parameter and the temperature of the observed region in the accretion column with the pulse phase.

A soft blackbody component might also be present in the pulse-phase–averaged spectrum as well as in the spectra corresponding to phase intervals 0–0.5 and 0.75–1. The temperature of this component in the pulse-phase–averaged spectrum is ~ 0.08 keV, corresponding to an unabsorbed luminosity of $\sim 1.6 \times 10^{37}$ ergs s^{-1}. The temperature seems to vary between ~ 0.03 keV at phases 0–0.5 and ~ 0.1 keV at phases 0.75–1. The radius of the spherical emission region of this component is between 400 and 2×10^4 km, well compatible with the magnetospheric radius of this source. In fact, considering a magnetic field of $1.8(1 + z) \times 10^{12}$ G (where z is the gravitational redshift) and a bolometric luminosity of $\sim 2.2 \times 10^{37}$ ergs s^{-1}, we find $R_M \sim 5 \times 10^3 \phi (1 + z)^{4/7}$ km, where ϕ is a correction factor that, in the case of disk accretion, is between 0.3 and 0.5 (see, e.g., Burderi et al. 1998; Ghosh & Lamb 1991). Therefore, this soft component can be emitted by the inner accretion disk at the magnetospheric radius or by matter at the magnetosphere (as in the case of Cen X-3, Burderi et al. 2000).

Finally, we analyzed eclipse spectra during the ingress, the deep eclipse, and the egress. The best fit to these spectra was obtained adopting the same model used for the out-of-eclipse spectrum multiplied by a partial covering. In this model the spectral evolution during the eclipse is explained by a progressive covering of the primary spectrum (or the part of it that is scattered into the line of sight), with both $N_{\rm Hpc}$ and $f_{\rm pc}$ increasing toward the deep eclipse. This model can fit both a soft excess and a prominent feature between 6 and 7 keV without the addition of extra emission components. In the deep eclipse we also find a softening of the power-law component. This could be caused by the increased contribution of the dust-scattered component, which has a softer spectrum (by $\sim E^{-2}$) relative to the incident spectrum (e.g., Day & Tennant 1991).

This work was supported by the Italian Space Agency (ASI) and by the Ministero della Ricerca Scientifica e Tecnologica (MURST).

REFERENCES

Becker, R. H., Swank, J. H., Boldt, E. A., Holt, S. S., Pravdo, S. H., Saba, J. R., & Serlemitsos, P. J. 1977, ApJ, 216, L11
Boella, G., Butler, R. C., Perola, G. C., Piro, L., Scarsi, L., & Blecker, J. 1997, A&AS, 122, 299
Brainerd, J. J., & Meszaros, P. 1991, ApJ, 369, 179
Bulik, T., Meszaros, P., Woo, J. W., Nagase, F., & Makishima, K. 1992, ApJ, 395, 564
Bulik, T., et al. 1995, ApJ, 444, 405
Burderi, L., Di Salvo, T., Robba, N. R., del Sordo, S., Santangelo, A., & Segreto, A. 1998, ApJ, 498, 831
Burderi, L., Di Salvo, T., Robba, N. R., La Barbera, A., & Guainazzi, M. 2000, ApJ, 530, 429
Clark, G. W., Woo, J. W., Nagase, F., Makishima, & K., Sakao, T. 1990, ApJ, 353, 274
Dal Fiume, D., et al. 2000, Adv. Space Res., 25(3), 399
Davison, P. J. N. 1977, MNRAS, 179, 35P
Day, C. S. R., & Tennant, A. F. 1991, MNRAS, 251, 76
Ebisawa, K., et al. 1996, PASJ, 48, 425
Ghosh, P., & Lamb, F. K. 1991, in Neutron Stars: Theory and Observation, ed. J. Ventura & D. Pines (NATO ASI Ser. C, 344; Dordrecht: Kluwer), 363
Makishima, K., Mihara, T., Nagase, F., & Tanaka, Y. 1999, ApJ, 525, 978
Meszaros, P., & Nagel, W. 1985a, ApJ, 298, 147
———. 1985b, ApJ, 299, 138
Mihara, T. 1995, Ph.D. thesis, Tokyo Univ.
Nagase, F., Corbet, R. H. D., Day, C. S. R., Inoue, H., Takeshima, T., Yoshida, K., & Mihara, T. 1992, ApJ, 396, 147
Robba, N. R., Cusumano, G., Orlandini, M., dal Fiume, D., & Frontera, F. 1992, ApJ, 401, 685
Rubin, B. C., Finger, M. H., Scott, D. M., & Wilson, R. B. 1997, ApJ, 488, 413
Rybicki, G. R., & Lightman, A. P. 1979, Radiative Processes in Astrophysics (New York: John Wiley & Sons)